EUROPEAN ORGANIZATION FOR NUCLEAR RESEARCH

DIRAC/PS212

CERN-EP-2018-281
04 November 2018

First measurement of a long-lived $\pi^+\pi^-$ atom lifetime

This paper is dedicated to the memory of our colleague Valeriy Yazkov who could not anymore see the full impact and significance of his contributions to the DIRAC experiment.

B. Adeva[1)], L. Afanasyev[2)], A. Anania[3)], S. Aogaki[4)], A. Benelli[5)], V. Brekhovskikh[6)], T. Cechak[5)], M. Chiba[7)], P. Chliapnikov[6)], P. Doskarova[5)], D. Drijard[8)], A. Dudarev[2)], D. Dumitriu[4)], D. Fluerasu[4)], A. Gorin[6)], O. Gorchakov[2)], K. Gritsay[2)], C. Guaraldo[9)], M. Gugiu[4)], M. Hansroul[8)], Z. Hons[10)], S. Horikawa[11)], Y. Iwashita[12)], V. Karpukhin[2)], J. Kluson[5)], M. Kobayashi[13)], V. Kruglov[2)], L. Kruglova[2)], A. Kulikov[2)], E. Kulish[2)], A. Lamberto[3)], A. Lanaro[14)], R. Lednicky[15)], C. Mariñas[1)], J. Martincik[5)], L. Nemenov[2,8)], M. Nikitin[2)], K. Okada[16)], V. Olchevskii[2)], V. Ovsiannikov[17)], M. Pentia[4)], A. Penzo[18)], M. Plo[1)], P. Prusa[5)], G. Rappazzo[3)], A. Romero Vidal[1)], A. Ryazantsev[6)], V. Rykalin[6)], J. Saborido[1)], J. Schacher[19,*)], A. Sidorov[6)], J. Smolik[5)], F. Takeutchi[16)], T. Trojek[5)], S. Trusov[21)], T. Urban[5)], T. Vrba[5)], V. Yazkov[21,†)], Y. Yoshimura[13)], P. Zrelov[2)]

DIRAC Collaboration

[1] Santiago de Compostela University, Spain
[2] JINR Dubna, Russia
[3] INFN, Sezione di Trieste and Messina University, Messina, Italy
[4] IFIN-HH, National Institute for Physics and Nuclear Engineering, Bucharest, Romania
[5] Czech Technical University in Prague, Czech Republic
[6] IHEP Protvino, Russia
[7] Tokyo Metropolitan University, Japan
[8] CERN, Geneva, Switzerland
[9] INFN, Laboratori Nazionali di Frascati, Frascati, Italy
[10] Nuclear Physics Institute ASCR, Rez, Czech Republic
[11] Zurich University, Switzerland
[12] Kyoto University, Kyoto, Japan
[13] KEK, Tsukuba, Japan
[14] University of Wisconsin, Madison, USA
[15] Institute of Physics ASCR, Prague, Czech Republic
[16] Kyoto Sangyo University, Kyoto, Japan
[17] Voronezh State University, Russia
[18] INFN, Sezione di Trieste, Trieste, Italy
[19] Albert Einstein Center for Fundamental Physics, Laboratory of High Energy Physics, Bern, Switzerland
[20] Basel University, Switzerland
[21] Skobeltsin Institute for Nuclear Physics of Moscow State University, Moscow, Russia
[*] Corresponding author.
[†] deceased

Abstract

The adapted DIRAC experiment at the CERN PS accelerator observed for the first time long-lived hydrogen-like $\pi^+\pi^-$ atoms, produced by protons hitting a beryllium target. A part of these atoms crossed the gap of 96 mm and got broken up in the 2.1 μm thick platinum foil. Analysing the observed number of atomic pairs, $n_A^L = 436^{+157}_{-61}\big|_{\rm tot}$, the lifetime of the $2p$ state is found to be $\tau_{2p} = (\,0.45^{+1.08}_{-0.30}\big|_{\rm tot}) \cdot 10^{-11}$s, not contradicting the corresponding QED $2p$ state lifetime $\tau_{2p}^{\rm QED} = 1.17 \cdot 10^{-11}$s. This lifetime value is three orders of magnitude larger than our previously measured value of the $\pi^+\pi^-$ atom ground state lifetime $\tau = (\,3.15^{+0.28}_{-0.26}\big|_{\rm tot}) \cdot 10^{-15}$s. Further studies of long-lived $\pi^+\pi^-$ atoms will allow to measure energy differences between p and s atomic states and so to determine $\pi\pi$ scattering lengths with the aim to check QCD predictions.

(To be submitted)

1 Introduction

The DIRAC collaboration aims to check low-energy QCD predictions using double-exotic $\pi^+\pi^-$ and $\pi^\pm K^\mp$ atoms, which have been observed and studied [1–7]. In strong inclusive processes, these atoms are produced in s states distributed according to n^{-3}, n being the principal quantum number [8].

The decay probability of short-lived $\pi^+\pi^-$ atoms ($A_{2\pi}$, pionium) in s states is dominated (99.6%) by the annihilation process [9–13]

$$\pi^+ + \pi^- \to \pi^0 + \pi^0 \tag{1}$$

and is given by the $\pi\pi$ s-wave scattering lengths combination $|a_0 - a_2|$ (a_I is the $\pi\pi$ scattering length for isospin I):

$$\frac{1}{\tau} \approx \Gamma(A_{2\pi} \to \pi^0\pi^0) = R\,|a_0 - a_2|^2 \quad \text{with} \quad R \propto |\psi_{nl}(0)|^2 . \tag{2}$$

The expression $\psi_{nl}(0)$ is the pure Coulomb atomic wave function at the origin with principal quantum number n and orbital quantum number l. The precision of the ratio R is 1.2% [13], and the scattering lengths and their combination have been calculated in low-energy QCD [14]: The lifetimes τ of the short-lived $\pi^+\pi^-$ and πK atoms in the ground state are about 3×10^{-15} s. The DIRAC experiment has measured these lifetimes and so derived combined $\pi\pi$ [1–3] and for the first time πK [5, 7] scattering lengths.

After investigation of $\pi\pi$ and πK atoms with "short" lifetimes of order 10^{-15}s, DIRAC continues its scientific program by exploring $\pi\pi$ atomic states ($A^L_{2\pi}$) of "long" lifetimes of order 10^{-11}s as considered in Ref. [8]. Moving inside the target, relativistic short-lived $A_{2\pi}$ interact with the electric field of the target atoms, resulting in a possible change of the $A_{2\pi}$ orbital momentum l by one or more units. Some (N^L_A) of them (N_A) will leave the target with $l > 0$. For excited states with $l \geq 1$, the decays of $A^L_{2\pi}$ into two π^0, $\pi^0 + \gamma$ and two γ are suppressed in accordance with (2) because of $|\psi_{nl}(0)|^2 = 0$. Therefore, the decay mechanism of such excited states is the radiative de-excitation to an ns state, annihilating subsequently with the "short" lifetime $\tau \cdot n^3$ into two π^0: The lifetimes of these long-lived states $A^L_{2\pi}$ are approximately given by the corresponding hydrogen de-excitation lifetimes (radiation transition) divided by the ratio of the reduced masses for $A_{2\pi}$ and hydrogen. The shortest $A^L_{2\pi}$ lifetime is the $2p$ state lifetime $\tau_{2p} \approx \tau^{\rm rad}_{2p} = 1.17 \cdot 10^{-11}$ s, which is three orders of magnitude larger than the minimum $A_{2\pi}$ lifetime. For an average momentum of detected $A_{2\pi}$ $\langle p_A \rangle$=4.44 GeV/c ($\gamma \simeq 15.9$), the decay lengths are 5.6 cm ($2p$), 18.4 cm ($3p$), 43 cm ($4p$), 83 cm ($5p$) and 143 cm ($6p$).

These large atom decay lengths in the laboratory (lab) system enable a measurement of the energy splitting between ns and np levels, $\Delta E^{ns-np} = E_{ns} - E_{np}$. By applying an electric or magnetic field, the Stark mixing of ns and np wave functions leads to a reduction of the long-lived atom lifetime depending on energy splitting and field strength. The lifetime dependence on energy splitting for static and periodic electric fields has been evaluated in [15, 16]. The energy shift (Lamb shift) of the levels with the principal quantum number n and orbital quantum number l is composed of the dominating strong contribution (80%) [17–19] and further contributions calculated precisely in QED [19–22]. The strong contribution for l=0 is related to the $\pi\pi$ scattering lengths [17, 19, 23] according to $\Delta E^{\rm str}_{n0} = A_n(2a_0 + a_2)$, where A_n is a known coefficient. The theoretical value of the $2s - 2p$ energy splitting amounts to $\Delta E^{2s-2p} = (-0.59 \pm 0.01)$ eV, whereas ΔE^{ns-np} decreases for higher n [19]. Hence, a measurement of ΔE^{ns-np} allows to obtain a value of the new combination of scattering lengths $2a_0 + a_2$.

In this paper, the DIRAC collaboration presents the first lifetime measurement of long-lived $\pi^+\pi^-$ atoms, observed by DIRAC as described in [23].

2 Setup for investigation of long-lived $\pi^+\pi^-$ atoms

To investigate long-lived $A_{2\pi}^L$ atoms, the primary 24 GeV/c CERN PS proton beam hits a 103 μm thick 99.98% pure Be target (Figures 1 and 2). A beam intensity of $3.0 \cdot 10^{11}$ protons per 450 ms spill [24] provides the needed $A_{2\pi}^L$ yield. The target thickness amounts to $3.0 \cdot 10^{-4}$ X_0 (radiation length), and the nuclear interaction probability is $\varepsilon_{nuc} = 2.5 \cdot 10^{-4}$. On their way to the Pt foil at a distance of 96 mm behind the Be target, a part of the produced long-lived atoms $A_{2\pi}^L$, depending on their lifetimes, decays, whereas the other part enters the Pt foil. By interacting with Pt atoms, the atoms $A_{2\pi}^L$ break up (get ionized) and generate atomic pairs with relative momenta Q <3 MeV/c in their pair centre-of-mass (c.m.) system. In addition, the proton beam interacting with the target (Figure 2) produces free (unbound) "Coulomb pairs" from short-lived sources as well as "non-Coulomb pairs" from long-lived sources and accidental coincidences (different proton-nucleus interactions). Therefore, the $A_{2\pi}^L$ signal, i.e. the corresponding atomic pairs, suffers from a $\pi^+\pi^-$ continuum background causing the main signal uncertainty.

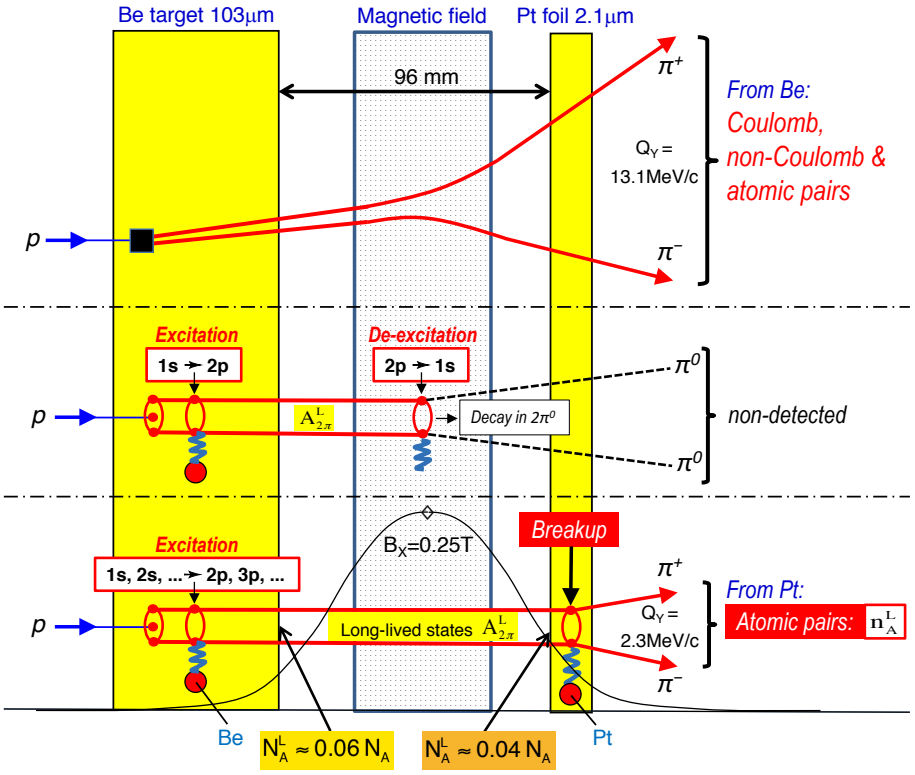

Fig. 1: Method to investigate long-lived $A_{2\pi}^L$ by means of a breakup foil (side view). N_A is the number of the totally produced $A_{2\pi}$ and N_A^L the number of excited $A_{2\pi}^L$ with $l > 0$.

The DIRAC setup [25], sketched in Figure 2, identifies pions, kaons, protons, electrons and muons by means of Cherenkov and preshower detectors, time-of-flight measurement and muon detectors. So, the huge e^+e^- bachground is 99.9% rejected [26]. The coordinate detectors and the vacuum channel allow to achieve a high resolution in the particle momentum determination ($\Delta p/p \simeq 3 \cdot 10^{-3}$) and so to measure Q of $\pi^+\pi^-$ pairs with the following precision: $\sigma_{QX} \approx \sigma_{QY} \approx 0.44$ MeV/c and $\sigma_{QL} \approx 0.50$ MeV/c. This high resolution enables the extraction of an atom signal in form of small Q atomic pairs. The secondary channel with the solid angle $\Omega = 1.2 \cdot 10^{-3}$ sr is vertically inclined relative to the proton beam by 5.7° upward. Downstream of the Be target, a 2.1 μm thick Pt foil ($6.9 \cdot 10^{-4}$ X_0, $\varepsilon_{nuc} = 0.23 \cdot 10^{-4}$) has been placed for $A_{2\pi}^L$ breaking up (ionization). The foil is introduced at 7.5 mm above the primary

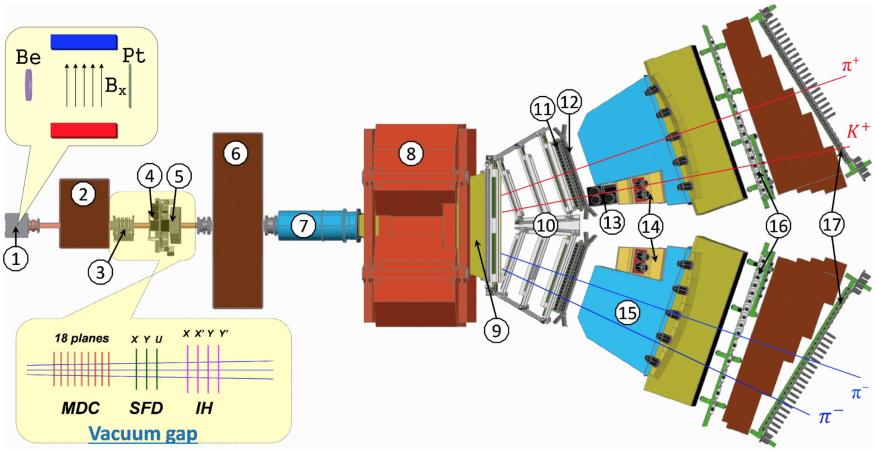

Fig. 2: Top view of the DIRAC setup: 1 – target station with insertion, showing the Be target, magnetic field and Pt breakup foil; 2 – first shielding; 3 – microdrift chambers (MDC); 4 – scintillating fiber detector (SFD); 5 – ionisation hodoscope (IH); 6 – second shielding; 7 – vacuum tube; 8 – spectrometer magnet; 9 – vacuum chamber; 10 – drift chambers (DC); 11 – vertical hodoscope (VH); 12 – horizontal hodoscope (HH); 13 – aerogel Cherenkov; 14 – heavy gas Cherenkov; 15 – nitrogen Cherenkov; 16 – preshower (PSh); 17 – muon detector. (The plotted symmetric and asymmetric events are a $\pi\pi$ and πK pair, respectively.)

proton beam to avoid interaction of the beam halo with Pt. The beam position in the vertical plane has been permanently monitored by checking the SFD and IH counting rates and by reconstructing the beam position with track information. Between target and breakup foil, there has been installed a permanent retractable magnet [27] with a pole distance of 60 mm (insertion of Figure 2) and a maximum horizontal field strength of 0.25 T (bending power 0.02 Tm): the magnet enlarges the value of the vertical component Q_Y of $\pi^+\pi^-$ pairs, generated in Be (Figure 1). By this means, the number of these pairs can be reduced in the low Q region, where the atomic pairs from the $A_{2\pi}^L$ breakup are expected. The Q_Y distribution, shifted by the magnetic field, for $\pi^+\pi^-$ pairs is shown in Figure 3. There are two peaks (Section 3): the first peak (right) is formed by Coulomb and atomic pairs produced in the Be target (Be peak) and the second one (left) by atomic pairs from long-lived atoms broken up in Pt (Pt peak). Initially, both peaks are at $Q_Y = 0$. Introducing the permanent magnet, the Be peak is shifted to $Q_Y = 13.1$ MeV/c and the Pt peak to $Q_Y = 2.3$ MeV/c, because these pairs pass different path lengths in the magnetic field. A strong drop in the distribution is induced for $Q_Y > 10$ MeV/c by the coplanarity cut in the trigger system [25]. This cut suppresses events with a vertical distance between two particles of more than 2 HH slabs ($\Delta Y > 51 \div 75$ mm), reducing the recording efficiency for $\pi^+\pi^-$ pairs with $Q_Y > 10$ MeV/c (Figure 3). This trigger influence on the peak position is removed in the ratio of prompt to accidental $\pi^+\pi^-$ pairs. In this distribution, the position of the Be peak is at $Q_Y = 13.15$ MeV/c (Figure 4a) and in the simulation at $Qy = 13.12$ MeV/c (Figure 4b), demonstrating good agreement.

An additional measurement of the Q_Y shift exploits in Be generated e^+e^- Dalitz pairs as well as such e^+e^- pairs, produced by photons in the Pt foil and traversing only the fringing magnetic field [23]. It is shown that Dalitz pairs get a ΔQ_Y shift of 12.9 MeV/c, compared to the shift of 2.3 MeV/c for e^+e^- pairs from Pt. This large difference in the Q_Y shift allows to suppress the background by a factor of about 6 in detecting atomic pairs from long-lived $A_{2\pi}^L$. The peak position for Dalitz pairs at $Q_Y = 12.9$ MeV/c has been used to control and measure the magnetic field stability during the 6 month data taking in 2012. The magnetic field strength is stable within a relative precision of better than $5 \cdot 10^{-4}$ [23]. The small difference in the peak position for $\pi^+\pi^-$ and e^+e^- pairs produced in Be is caused by higher ionization and radiation losses of e^+e^-.

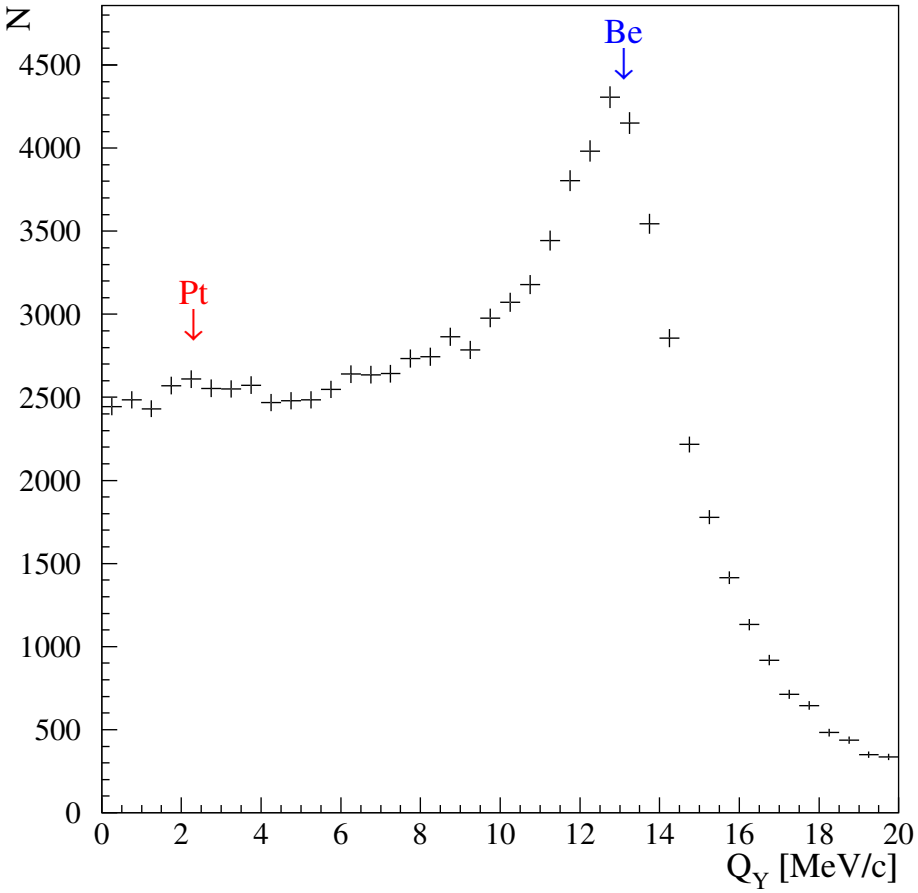

Fig. 3: Experimental Q_Y distribution of $\pi^+\pi^-$ pairs. The data are selected with the criteria $|Q_X| < 2$ MeV/c and $|Q_L| < 2$ MeV/c. The first big peak (right) is formed by Coulomb and atomic pairs from the Be target and the second one (left) by atomic pairs from the Pt foil. These peaks are shifted to different values of Q_Y, because the $\pi^+\pi^-$ pairs from Be and those from Pt pass different segments of the permanent magnet field.

3 Generation of short-lived $\pi^+\pi^-$ atoms, Coulomb and non-Coulomb pairs

Prompt oppositely charged $\pi^+\pi^-$ pairs, emerging from proton-nucleus collisions, are produced either directly or indirectly, originating from short-lived (e.g. Δ, ρ), medium-lived (e.g. ω, ϕ) or long-lived sources (e.g. η', η). These pion pairs, except those from long-lived sources, undergo Coulomb final state interaction (FSI) resulting in modified unbound states or bound systems. These atomic states are formed in s states with a known distribution of the principal quantum number [8]. Pairs from long-lived sources are nearly unaffected by the Coulomb interaction. The accidental pairs arise from different proton-nucleus interactions.

The cross section of $\pi^+\pi^-$ atom production is given in [8] by the expression:

$$\frac{d\sigma_A^n}{d\vec{p}_A} = (2\pi)^3 \frac{E_A}{M_A} \left.\frac{d^2\sigma_s^0}{d\vec{p}_+ d\vec{p}_-}\right|_{\vec{p}_+\approx\vec{p}_-} \cdot |\psi_n(0)|^2 = (2\pi)^3 \frac{E_A}{M_A} \frac{1}{\pi a_B^3 n^3} \left.\frac{d^2\sigma_s^0}{d\vec{p}_+ d\vec{p}_-}\right|_{\vec{p}_+\approx\vec{p}_-}, \qquad (3)$$

where $\vec{p}_A$, E_A and M_A are the momentum, energy and rest mass of the $A_{2\pi}$ atom in the lab system, respectively, $\vec{p}_+$ and $\vec{p}_-$ the momenta of the charged pions and a_B the corresponding Bohr radius. The inclusive production cross section of $\pi^+\pi^-$ pairs from short-lived sources without FSI is denoted by σ_s^0, and $\psi_n(0)$ is the s state atomic Coulomb wave function at the origin with the principal quantum number n. According to (3), $\pi^+\pi^-$ atoms are produced only in s states with probabilities $W_n = \frac{W_1}{n^3}$: $W_1 = 83.2\%$, $W_2 = 10.4\%$, $W_3 = 3.1\%$, $W_{n>3} = 3.3\%$. In complete analogy, the production of free

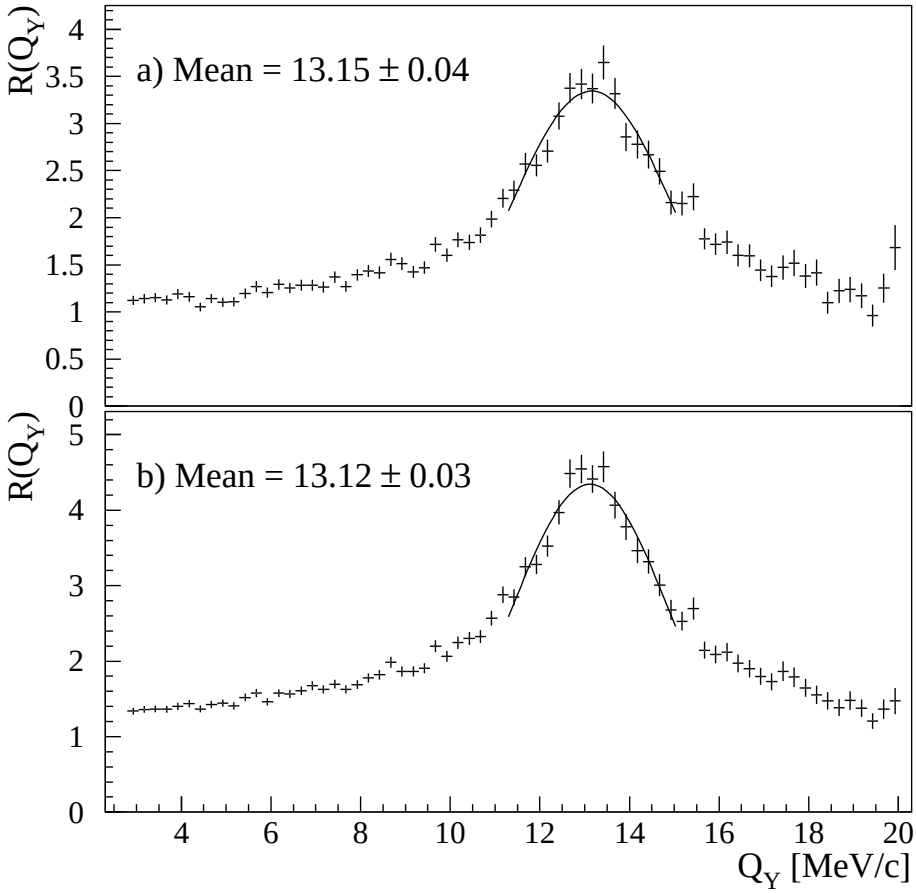

Fig. 4: Ratio $R(Q_Y)$ of prompt to accidental $\pi^+\pi^-$ pairs. Top: Experimental distribution. The peak at $Q_Y = 13.15$ MeV/c corresponds to the Coulomb pairs produced in the Be target. Bottom: Simulated distribution. Gaussian fits are applied to get precise peak positions.

oppositely charged $\pi\pi$ pairs from short- and medium-lived sources, i.e. Coulomb pairs, is described in the pointlike production approximation by

$$\frac{d^2\sigma_C}{d\vec{p}_+ d\vec{p}_-} = \frac{d^2\sigma_s^0}{d\vec{p}_+ d\vec{p}_-} A_C(q) \quad \text{with} \quad A_C(q) = \frac{2\pi m_\pi \alpha/q}{1-\exp\left(-2\pi m_\pi \alpha/q\right)} \,. \tag{4}$$

The Coulomb enhancement function $A_C(q)$ (q is the pair c.m. relative momentum at the production point) is the well-known Gamov-Sommerfeld-Sakharov factor [28–30]. The relative yield between atoms and Coulomb pairs [31] is given by the ratio of equations (3) and (4). The total number N_A of produced $A_{2\pi}$ is determined by the model-independent relation

$$N_A = K(q_0) N_C(q \le q_0) \quad \text{with} \quad K(q_0 = 2 \text{ MeV}/c) = 0.615 \,, \tag{5}$$

where $N_C(q \le q_0)$ is the number of Coulomb pairs with $q \le q_0$ and $K(q_0)$ a known function of q_0.

Up to now, the pair production is assumed to be pointlike. In order to check finite size effects due to the presence of medium-lived resonances (ω, ϕ), a study about non-pointlike particle pair sources has been performed [32, 33]. Because of the large Bohr radius $a_B = 387$ fm, the pointlike treatment of the Coulomb $\pi\pi$ FSI is valid for directly produced pairs as well as for pairs from short-lived strongly decaying resonances. This treatment, however, should be adjusted for pions originating from decays of medium-lived particles with path lengths comparable with a_B in the c.m. system. Corrections to the pointlike Coulomb FSI can be performed by means of the two correction factors $1+\delta(q)$ and $1+\delta_n$ (n

is the principal quantum number), which have to be applied to the calculated pointlike production cross sections of Coulomb $\pi^+\pi^-$ pairs (4) and s state $\pi^+\pi^-$ atoms (3), correspondingly [32, 33].

4 Production of long-lived $\pi^+\pi^-$ atoms

The short-lived $\pi^+\pi^-$ atoms, which propagate in the Be target after their production in ns states, are either decaying or interacting with Be. This interaction with the electric field of target atoms will exite/de-excite or break up $\pi^+\pi^-$ atoms. In the excitation/de-excitation processes, only transitions with Z-parity ($P^Z = (-1)^{l+m}$) conservation are permitted [34], changing the orbital momentum by one unit or more and so forming long-lived atoms. The quantization axis is along the lab atom momentum. The lifetime of $\pi^+\pi^-$ atoms in the lab system depends on the quantum numbers n,l and the atom momentum. The populations of the atomic states with quantum numbers n,l,m are described by an infinite set of transport equations in terms of probabilities [35, 36]. These equations account for excitation/de-excitation and annihilation processes and describe the atomic state populations from the production point up to the target exit. For the calculations below, our measured value of the $A_{2\pi}$ ground state lifetime $\tau = 3.15 \cdot 10^{-15}$s [3] and the atom lab momentum spectrum, extracted from the experimental Coulomb pair distribution (Figure 5), are used.

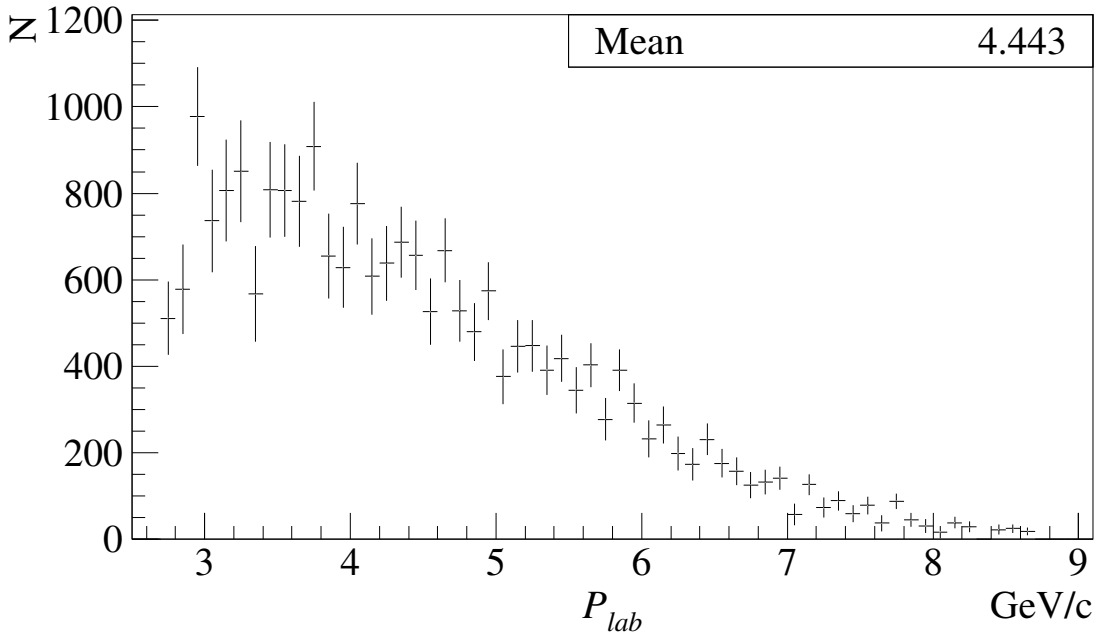

Fig. 5: Lab momentum spectrum of $A_{2\pi}$ produced in Be, as used in the simulation.

4.1 Population of long-lived states

In this paper, the transport equations are solved numerically for all states with principal quantum numbers $n \leq 10$. The populations of states with higher n are taken into account by an extrapolation procedure. Only total and excitation/de-excitation cross sections are considered: the cross sections are calculated in the first Born approximation (one-photon exchange), using Molière parametrization of the Thomas-Fermi formfactors for Be and Pt atoms. Its main advantage is a possibility to get exact numerical solutions for higher n. Some atomic state populations at the Be target exit are presented in Table 1. The population is given in % of the total number N_A of produced atoms. The Z-parity conservation reduces the number of populated states, taking into account that the atoms are initially produced only in ns states.

Figure 6 shows the atomic state population P_n^L versus n, summed over l and m at the exit of the Be target and before the Pt foil. The almost pure exponential behaviour at high n allows to extrapolate to

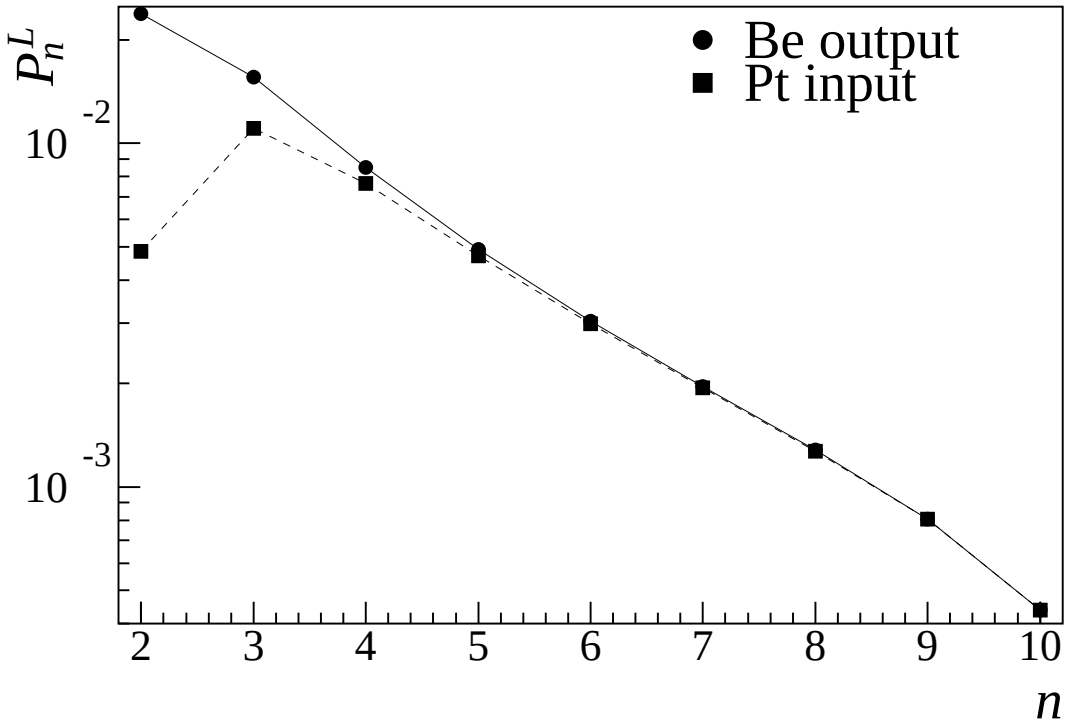

Fig. 6: Populations P_n^L of long-lived states $A_{2\pi}^L$ versus n, summed over l and m, at the exit of the Be target (•) and at the Pt foil entry (■).

$n > 10$ and to evaluate the population of the non-negligible infinite "tail". Thus, the population of all discrete states can be estimated. The population at $n = 10$ is excluded from the extrapolation procedure, as this population is underestimated because of cutting the infinite set of transport equations, excluding de-excitations to this state from higher n states. The cut does almost not affect the populations with smaller n, as transitions between nearest n levels dominate. A fitting procedure over all points is badly suited for the "tail" estimation, as the n dependence is mainly dictated by two different dependences: production rates as n^{-3} and total cross sections roughly as n^2. The following two n dependences are chosen for extrapolation: exponential, $a\exp(-bn)$, and hyperbolic, $cn^{-3} + dn^{-5}$. The free parameters a, b and c, d have been calculated for n, using the populations P_n^L and P_{n-1}^L.

Figure 7 illustrates the "tail" estimations. The numerical solution of the transport equations are obtained for $n \leq 10$. Then, the populations at $n = 9$ and 8 are used for the "tail" estimation. The two upper points at $n = 9$ in Figure 7 show the sum of the populations for $n \leq 9$ plus the different "tail" estimations (exponential – •, hyperbolic – ▲). The lower point (■) presents the sum of the populations with $n \leq 9$ plus the population for $n = 10$ instead of the "tail". The curves are obtained by applying the same procedure to the points with lower n. The exponential "tail" estimation is chosen as the mean value for the population of long-lived states, as it has the smallest slope and is nearly flat for $n \geq 7$. The two other curves are used as error band. The illustrative numerical values are calculated for the average atom momentum $\langle p_A \rangle = 4.44$ GeV/c (Figure 5): the sum of the long-lived state population at the Be exit is 6.04% for $n \leq 10$ (5.99% for $n \leq 9$) of the total number N_A of produced $A_{2\pi}$; the exponential "tail" $n \geq 10$ is 0.14%, the hyperbolic "tail" 0.25%, and the population of all long-lived states at the Be exit is given as $N_A^{L,\mathrm{Be}} = (6.13^{+0.11}_{-0.09}) \cdot 10^{-2} \times N_A$. Moreover, about 17% of $A_{2\pi}$ are produced in short-lived states (ns) and annihilate just behind the Be target. About 4.6% of the atoms break up in Be producing atomic pairs. Let us underline that accuracy of all above numbers accounts for the accuracy of the extrapolation procedure.

As mentioned above, the cut of the infinite set of transport equations at $n \leq 10$ leads to a small under-

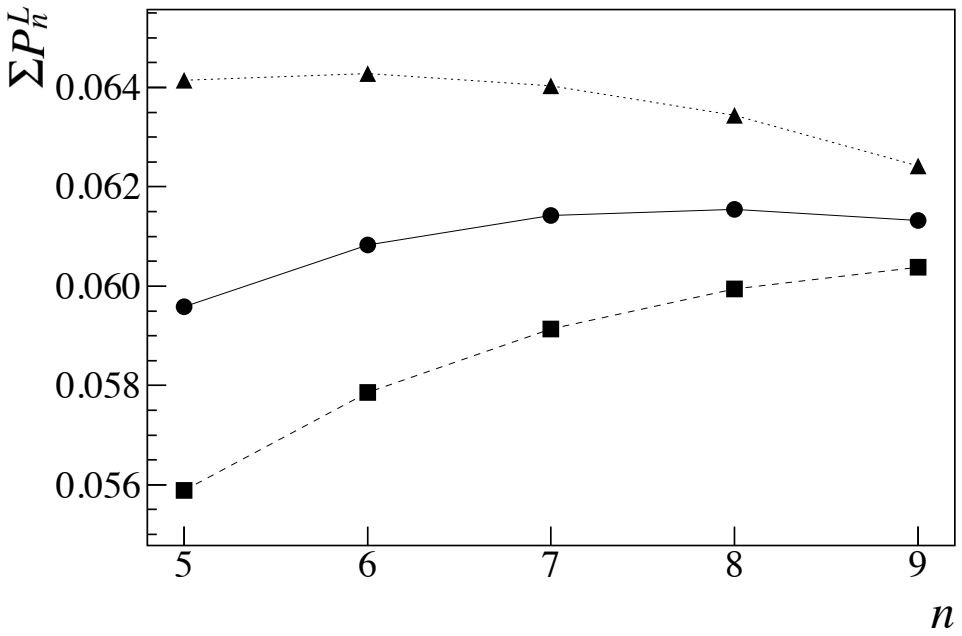

Fig. 7: Summed populations $\sum P_n^L$ of all long-lived atomic states at the exit of the Be target as a function of n used for "tail" estimation. For each n, the two upper curves show the sum of state populations for the given n plus different "tail" estimations calculated from populations for n and $n-1$ (exponential "tail" – •, hyperbolic "tail" – ▲). The lower curve (■) presents the sum of the population for the given n plus the population for $n+1$ instead of the "tail".

estimation of all low-lying states because of neglecting the de-excitation from the truncated "tail" with $n > 10$. A possible influence of this cut has been estimated by comparing the above solution with a solution, cut at $n \leq 9$, where the de-excitation from states with $n = 10$ are also truncated. The differences of all populations calculated for $n \leq 10$ and $n \leq 9$ have been used to estimate the contribution of the truncated "tail" to the low-lying states. As the populations of all states with $n = 10$, $P_{10} = 0.044\%$, is 2.15 times smaller than the "tail" with $n > 10$, $P_{tail} = 0.094\%$, the influence of the "tail" is expected to be 2.15 times larger. Thus, the corrected populations are calculated as a sum of the populations with the cut $n \leq 10$ plus the corresponding differences multiplied by 2.15. This modifies the summed populations of long-lived states by only 1‰ for $n = 2$–5 and by 9‰ for $n = 2$–9. Then, these corrected populations are used in the extrapolation procedure described above. Because the accuracy of the corrections quickly decreases for n near the cut value, the exponential extrapolation at $n = 7$, lying in the middle of the plateau in Figure 7, is chosen as mean value. The error band is set very conservatively: the "minus" error from the exponential extrapolation at $n = 6$, the "plus" error from the hyperbolic extrapolation at $n = 8$. This way, the population of long-lived states at the Be exit is $(6.29^{+0.33}_{-0.13}) \cdot 10^{-2}$.

An additional correction to this value may arise from the accuracy of atom-atom cross sections. The most accurate cross sections are obtained in the Glauber approach accounting for multi-photon exchange and the Hartree-Fock-Dirac form factors of the target atoms [38–40]. Unfortunately, these cross sections are only available for $n \leq 8$. As shown in [37], the accuracy of the used cross sections, compared to the most accurate ones, depends on the target material. The $A_{2\pi}$ breakup probability in the 95 μm Nickel target calculated with these cross sections is by 2.9% smaller than calculated with the most accurate cross sections. For a 28 μm Pt target, the breakup probability is by 3% larger [37]. In the case of the Be target,

an estimation shows that the difference has the same scale. The summed population of long-lived states for $n \leq 8$ at the Be exit, calculated with the most accurate cross sections, is 2.8% less than the current value. Thus, this value can be used as the scale factor accounting for uncertainties of the used atom-atom cross sections. Further, the accuracy of the most accurate cross sections is estimated to be about 1% [38–40], which can be converted roughly to a 1% error in the populations. Let us conservatively add this error linearly to the latter error band. Finally, the population of long-lived states at the Be exit is $(6.12^{+0.39}_{-0.19}) \cdot 10^{-2}$, compared to $(6.13^{+0.11}_{-0.09}) \cdot 10^{-2}$ in the above calculations. Thus, this crude accuracy estimation leads mainly to an increase of the error band for the calculated probabilities. Nevertheless, it is significantly smaller than the experimental error. Hence, its influence is applied only to the final results as described below.

4.2 Decay in gap and breakup in Pt for long-lived atoms

In the 96 mm gap between the Be target and the Pt foil, the populations of the atomic states alter depending on their lifetime [43], calculated in QED (Figure 8). The decay length of atoms with fixed n is minimal for $l = 1$ and strongly increasing with l. As shown in Section 1, these values increase from 5 cm to 1 m with n. Figure 6 indicates that mainly states with $n = 2-4$ are decaying in the gap. The summed population of long-lived states at the entry of the Pt foil is 0.037 ± 0.001. Note that all cascade radiation transitions between atomic states as well as annihilation of ns states are considered, using the technique of transport equations. The cascade accounting increases the summed population by about 10% compared to a pure exponential decay.

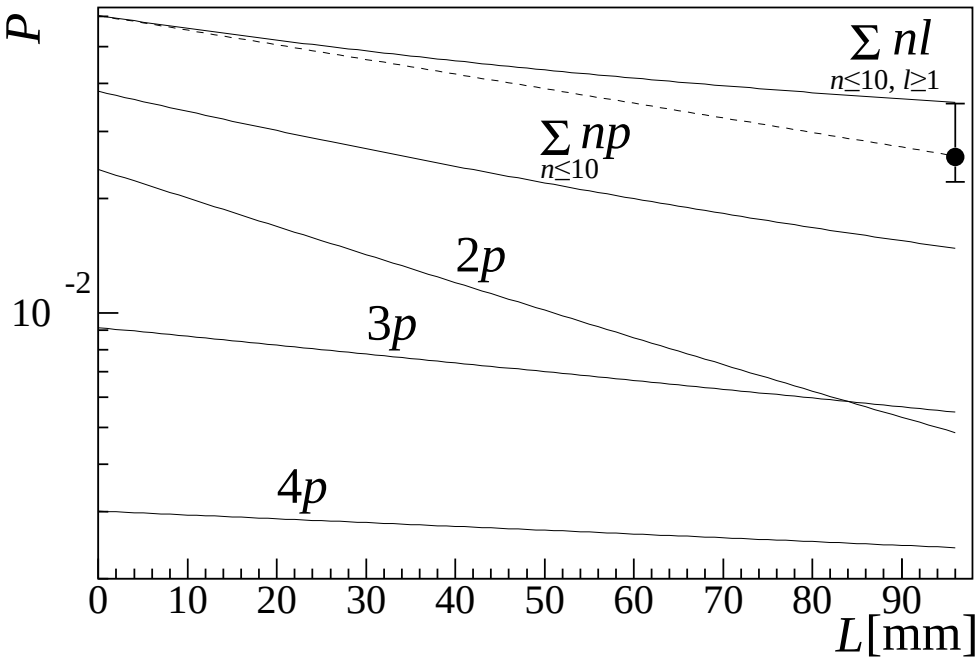

Fig. 8: Decrease of the atomic state populations in the 96 mm gap between the Be target and the Pt foil on the basis of QED lifetimes for long-lived atomic states. The point with the error bar corresponds to our measured value (8). The straight dashed line illustrates the simplified approach that all long-lived states decrease, as a single state, exponentially (9).

Table 2 shows the summed populations of long-lived states at the Be target exit and at the Pt foil entry as a function of n. Illustrative values of np state breakup probabilities in the Pt foil are shown as well. The pionium breakup in Pt is treated in the same way as the breakup in the target: the transport equations use all cross sections for the pionium interaction with Pt, state populations and pionium annihilation. The breakup probability of $A^L_{2\pi}$ entering in Pt, averaged over populations, is 0.944.

Table 1: Population P of atomic states with the quantum numbers n, l and m at the exit of the 103 μm thick Be target. The calculations are performed for the average atom momentum 4.44 GeV/c and the ground state lifetime $\tau = 3.15 \cdot 10^{-15}$s. $\sum_m$ is the population summed over the quantum number m, and $\sum_{l,m}^{L}$ the long-lived state population summed over l and m. All numbers are given in % of the total number N_A of produced atoms.

n	l	m	P	$\sum_m$	$\sum_{l,m}^{L}$
1	0	0	11.84	11.84	
2	0	0	4.08	4.08	
	1	−1 , 1	2×1.19	2.38	2.38
3	0	0	0.78	0.78	
	1	−1 , 1	2×0.46	0.91	1.56
	2	−2 , 2	2×0.26	0.65	
		0	0.12		
4	0	0	0.21	0.21	
	1	−1 , 1	2×0.15	0.30	0.85
	2	−2 , 2	2×0.12	0.29	
		0	0.06		
	3	−3 , 3	2×0.09	0.25	
		−1 , 1	2×0.038		
5	0	0	0.075	0.075	
	1	−1 , 1	2×0.058	0.116	0.49
	2	−2 , 2	2×0.060	0.128	
		0	0.028		
	3	−3 , 3	2×0.044	0.128	
		−1 , 1	2×0.020		
	4	−4 , 4	2×0.038	0.119	
		−2 , 2	2×0.015		
		0	0.012		
6	0	0	0.032	0.032	
	1	−1 , 1	2×0.026	0.052	0.30
	2	−2 , 2	2×0.023	0.061	
		0	0.014		
	3	−3 , 3	2×0.022	0.065	
		−1 , 1	2×0.011		
	4	−4 , 4	2×0.020	0.065	
		−2 , 2	2×0.0088		
		0	0.0071		
	5	−5 , 5	2×0.018	0.062	
		−3 , 3	2×0.0074		
		−1 , 1	2×0.0055		

n	l	m	P	$\sum_m$	$\sum_{l,m}^{L}$
7	0	0	0.015	0.015	
	1	−1 , 1	2×0.013	0.026	0.19
	2	−2 , 2	2×0.012	0.031	
		0	0.007		
	3	−3 , 3	2×0.011	0.034	
		−1 , 1	2×0.0058		
	4	−4 , 4	2×0.011	0.035	
		−2 , 2	2×0.0049		
		0	0.0041		
	5	−5 , 5	2×0.010	0.035	
		−3 , 3	2×0.0043		
		−1 , 1	2×0.0033		
	6	−6 , 6	2×0.0095	0.035	
		−4 , 4	2×0.0038		
		−2 , 2	2×0.0027		
		0	0.0024		
8	0	0	0.008	0.008	
	1	−1 , 1	2×0.0068	0.014	0.12
	2	−2 , 2	2×0.0063	0.016	
		0	0.0038		
	3	−3 , 3	2×0.0061	0.019	
		−1 , 1	2×0.0032		
	4	−4 , 4	2×0.0058	0.020	
		−2 , 2	2×0.0028		
		0	0.0023		
	5	−5 , 5	2×0.0056	0.020	
		−3 , 3	2×0.0025		
		−1 , 1	2×0.0019		
	6	−6 , 6	2×0.0054	0.020	
		−4 , 4	2×0.0023		
		−2 , 2	2×0.0016		
		0	0.0015		
	7	−7 , 7	2×0.0051	0.020	
		−5 , 5	2×0.0021		
		−3 , 3	2×0.0014		
		−1 , 1	2×0.0012		

Finally, the expected total probability $P_{\rm br}^{\rm tot}({\rm Pt})$, that pionium produced in Be will break up in Pt, is calculated via the difference between the total populations at the entry and exit of the Pt foil. For the average atom momentum (see above), this probability is found to be:

$$P_{\rm br}^{\rm tot}({\rm Pt}) = 0.035 \pm 0.001 \; . \tag{6}$$

Table 2: Summed (over l and m) populations of long-lived atomic states versus n. The populations at the Be target exit and at the Pt foil entry are given in % of the total number of produced $A_{2\pi}$. $P_{\rm br}^{\rm Pt}(np)$ is the breakup probability of the $A_{2\pi}$ np states in the 2.1 μm thick Pt foil. The values are calculated for the average atom momentum 4.44 GeV/c and the ground state lifetime $\tau = 3.15 \cdot 10^{-15}$s.

n	2	3	4	5	6	7	8
Be	2.38	1.56	0.85	0.49	0.30	0.20	0.13
Pt	0.48	1.10	0.76	0.47	0.30	0.19	0.13
$P_{\rm br}^{\rm Pt}(np)$	0.763	0.933	0.978	0.991	0.996	0.998	0.999

The magnetic field in the lab system between the Be target and the Pt foil transforms into an electric field perpendicular to the atom momentum in the atom c.m. system. This electric field mixes the wave functions of long-lived np states with $m = \pm 1$ and short-lived ns states of the same principal quantum number n. Thus, the lifetime of long-lived atoms will decrease, depending on n, the electric field strength and the energy splitting between mixing states. The states nl of higher orbital momenta $l > 1$ may also be mixed with ns states, but only in higher order of the electric field. Therefore, the variation of their lifetimes may be neglected compared with that of the np states. The influence of the magnetic field on the lifetime has been evaluated in [15] for $2p$ and $2s$ states, only. The magnetic field in the gap shortens the $2p$ lifetime by 1.002. For higher n, the influence of the magnetic field on the np lifetime will increase. As seen from Table 1, the population of $m = \pm 1$ states decreases with increasing n. If all npm states with $n = 4$–10 and $m = \pm 1$ will annihilate, then the number of long-lived atoms at the Pt foil entry will be reduced by approximately 8.6%. This value may be considered as a maximal estimate for the impact of the magnetic field on the population of long-lived states.

5 Simulation of Coulomb, non-Coulomb and atomic pairs

The pair and atom simulation is performed in the framework of the DIPGEN code [42].

1. Non-Coulomb $\pi^+\pi^-$ pairs, not affected by FSI, are distributed in q in accordance with phase space $\propto q^2$. For Coulomb pairs, which are exposed to Coulomb FSI, the q distribution is modified by the Gamov-Sommerfeld-Sakharov factor (4). The Monte Carlo (MC) distributions of the lab pair momentum are based on the experimental momentum distribution of Coulomb and non-Coulomb pairs. In first approximation, the $\pi^+\pi^-$ Coulomb pairs are simulated according to $dN/dp = \exp(-0.4066 + 0.2864p)$ with p in GeV/c. After comparison of the experimental with the MC distribution as reconstructed by the DIRAC program ARIANE, the simulated distribution is adapted by applying a weight function to fit the experimental data. Figure 5 presents the lab momentum distribution of produced atoms, reconstructed from the spectrum of detected Coulomb pairs.

2. Pionium propagation in the Be target between the production and the breakup point in Be or in the Pt foil from the entry to the breakup point is simulated by transport equations. In the framework of the DIPGEN code [42], the interaction between pionium and target atoms is described by the cross sections published in [38–40]. Thus, the populations of the atomic states before the breakup are accurately accounted for. The distributions of the relative momentum q of atomic pairs as produced in Be or Pt are generated according to the spectra of pairs from atom breakup by taking into account their quantum numbers.

3. In the simulation, atomic pairs from $A_{2\pi}^{L}$ breakup as well as Coulomb, non-Coulomb and atomic pairs generated in Be propagate through the setup according to the programs GEANT-DIRAC (setup) and ARIANE (reconstruction). The description of the charged particle propagation includes (a) multiple scattering in the target, the magnetic field and multiple scattering in Pt, detector planes and setup partitions and (b) the response of the detectors and (c) the additional momentum smearing.

4. The influence of the permanent magnet field between Be and Pt is taken into account with the same technique and accuracy as the field of the spectrometer magnet. The quality of this description is illustrated in Figure 4.

6 Event reconstruction

The events are reconstructed by means of the DIRAC $\pi\pi$ analysis software described in [23].
1. Only events with one or two so-called DC tracks – tracks reconstructed only with DC hits – in each arm are processed.
2. The DC tracks are extrapolated backward to the incident proton beam position on the target, using the inverse transfer function of the DIRAC dipole magnet. This procedure provides a first approximation of the particle momenta and the corresponding intersection points in MDC, SFD and IH.
3. SFD hits are searched for in a square of side length ± 1 cm, corresponding to 3σ (5σ) for low (high) momentum particles. If the number of hits around the two tracks is $\leq$4 in each SFD plane and $\leq$9 in all three SFD planes, the event is kept.
4. The momenta of the positively and negatively charged particles are modified to match the DC track X-coordinates and the SFD hits in the X- or U-plane. In the final analysis, the combination with the best χ^2 in the SFD planes and target vertex is selected.

The setup is aligned, using properties of Λ ($\bar{\Lambda}$) decays [44]. The decay particles are reconstructed and the corresponding invariant mass determined. After alignment, the experimental and simulated values of the Λ mass coincide with the PDG value within 6 digits. The resolution in the components of the relative pair momentum Q, excluding target multiple scattering, are as follows [23]: $\sigma(Q_X) = \sigma(Q_Y) = 0.44$ MeV/c and $\sigma(Q_L) = 0.50$ MeV/c.

7 Measuring the number of produced atoms in the Be target

The analysis of $\pi^+\pi^-$ experimental data, produced in the Be target, is similar to the $\pi^+\pi^-$ analysis as presented in [3]. The main difference is a shift in Q_Y by 13.1 MeV/c, due to the magnetic field of the inserted permanent magnet. For the analysis in the current section, the found Q_Y value of each experimental and MC event is lessened by the above 13.1 MeV/c.

Events with transverse $Q_T < 4$ MeV/c and longitudinal $|Q_L| < 15$ MeV/c are selected to be analysed. The experimental Q-distribution $N(Q_i)$ and the distributions of its projections are fitted by simulated distributions of atomic $n_A^{MC}(Q_i)$, Coulomb $N_C^{MC}(Q_i)$ and non-Coulomb $N_{nC}^{MC}(Q_i)$ pairs. Using the difference of the particle production times, the admixture of accidental pairs is subtracted from the experimental distributions. The distributions of simulated events, $n_A^{MC}(Q_i)$), $N_C^{MC}(Q_i)$ and $N_{nC}^{MC}(Q_i)$, are normalized to 1. In the experimental distributions, the numbers of atomic (n_A), Coulomb (N_C) and non-Coulomb (N_{nC}) pairs are free fit parameters in the minimizing expression:

$$\chi^2 = \sum_i \frac{(N(Q_i) - n_A \cdot n_A^{MC}(Q_i) - N_C \cdot N_C^{MC}(Q_i) - N_{nC} \cdot N_{nC}^{MC}(Q_i))^2}{\sigma_{N(Q_i)}^2}. \quad (7)$$

The sum of these parameters is equal to the number of analysed events. The fitting procedure takes into account the statistical errors of the experimental distributions.

Figure 9 shows the experimental and simulated Q_L distributions of $\pi^+\pi^-$ pairs for the data obtained from the Be target. One observes a very good agreement of the sum of simulated Coulomb and non-Coulomb pairs with experimental data in the region of $Q_L > 1.5$ MeV/c, where no atomic pairs are expected. The main result of this fit is the number of Coulomb pairs: using (5), this number allows to obtain the full number of $\pi^+\pi^-$ atoms produced in the Be target.

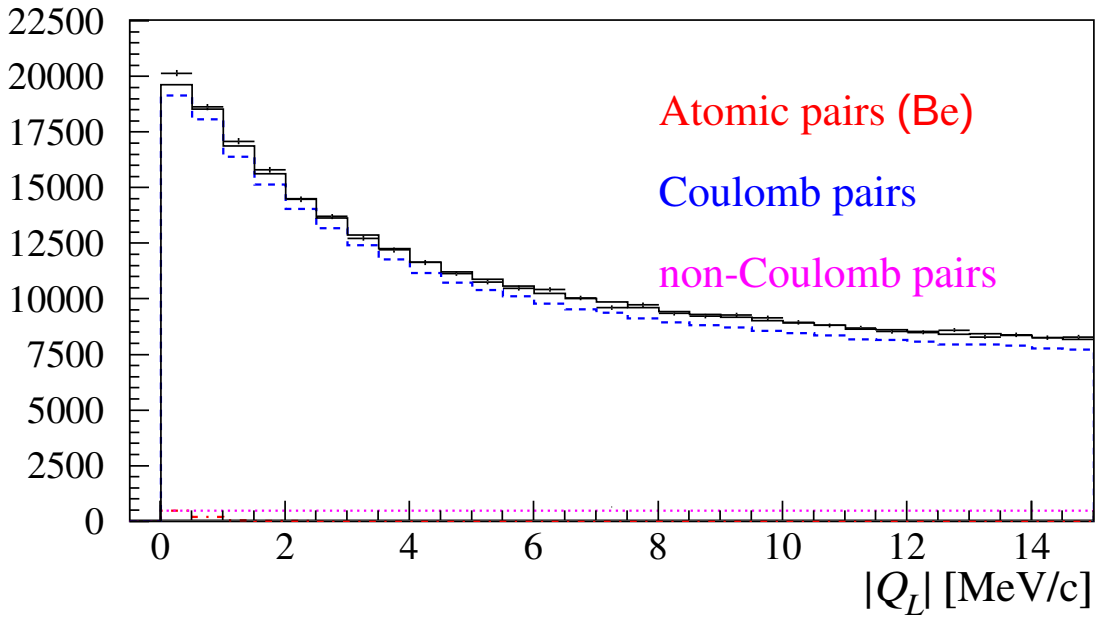

Fig. 9: Experimental Q_L distribution of $\pi^+\pi^-$ pairs (+ with error bar) for the beryllium (Be) target fitted by the sum of simulated distributions of "atomic", "Coulomb" and "non-Coulomb" pairs. The summed distribution of free ("Coulomb" and "non-Coulomb") pairs is shown as black line.

The Coulomb pairs from this distribution are used to reconstruct the lab momentum of produced atoms, shown in Figure 5. The average momentum is $\langle p_A \rangle = 4.44$ GeV/c. This spectrum is used in the atom simulation. Atomic pairs from $A^L_{2\pi}$ breakup exhibit almost the same spectrum, but – due to Lorentz boost – with a small shift to higher momentum with an average momentum of $\langle p_A \rangle = 4.59$ GeV/c.

Table 3 summarizes the number of Coulomb pairs N_C from the 1-dimensional Q and $|Q_L|$ analyses and from the 2-dimensional ($|Q_L|$,Q_T) analysis. The efficiency of Coulomb pair recording is evaluated from the simulated data as ratio of the MC Coulomb pair number N_C^{MC}, passing the corresponding cuts — in each of the above analyses — to the full number of generated Coulomb pairs $N_C^{MC}(0)$: $\varepsilon_C = N_C^{MC}/N_C^{MC}(0)$. The full number of produced Coulomb pairs in the Be target is then given by N_C/ε_C. This number allows to calculate the number N_A of atoms produced in the Be target: using the theoretical ratio $K = N_A/N_C$ (5), calculated for $q \leq 2$ MeV/c, and the simulated probability $\varepsilon_K = N_C^{MC}(K)/N_C^{MC}(0)$, that the Coulomb pairs have momenta $q \leq 2$ MeV/c, results in $N_A = K \cdot \varepsilon_K \cdot N_C/\varepsilon_C$. To recover the losses due to the coplanarity cut in the trigger system (Section 2 and Figure 3), the number N_A is additionally corrected (MC). The corrected values $N_A^{\rm tot}$ are shown in the last column of Table 3.

8 Number of the long-lived atoms broken up in Pt

Atomic pairs from the $A^L_{2\pi}$ atom breakup in the Pt foil are observed [23] above background $\pi^+\pi^-$ pairs produced mainly in the Be target. For the analysis, the same approach is applied as in Section 7, but this time Q_Y is shifted by 2.3 MeV/c for all pairs instead of 13.1 MeV/c (Figures 1 and 3).

In the 2-dimensional $(|Q_L|, Q_T)$ analysis, experimental data are analysed by means of corresponding simulated distributions. For $|Q_L| < 15$ MeV/c and $Q_T < 2$ MeV/c, the $|Q_L|$ projection of the experimental

Table 3: Number N_C of Coulomb pairs from different analyses and fit quality as χ^2/n (n is degree of freedom). N_A is the corresponding number of atoms produced in the Be target and $N_A^{\rm tot}$ the total number of atoms after correction for the coplanarity cut. The errors are statistical ones.

Analysis	N_C	χ^2/n	N_A	$N_A^{\rm tot}$
Q	321340 ± 2660	33/27	12539 ± 97	17000 ± 130
$\lvert Q_L\rvert$	315830 ± 3250	30/27	12320 ± 120	16700 ± 160
$\lvert Q_L\rvert, Q_T$	319890 ± 2610	152/117	12483 ± 97	16960 ± 130

2-dimensional distribution as well as of the three types of simulated $\pi^+\pi^-$ pairs is shown in Figure 10a. One observes an excess of events – above the sum of Coulomb and non-Coulomb pairs – in the low Q_L region, where atomic pairs are expected. After background subtraction, there is a statistically significant signal of $n_A^L = 436 \pm 57$ as presented in Figure 10b. The signal shape is compared with the simulated distribution of atomic pairs resulting from the $A_{2\pi}^L$ breakup in the Pt foil. The description is acceptable in view of large statistical uncertainties induced by subtracting two large numbers in the bins of the signal distribution (see discussion below). Figure 11a presents the Q_T projection of the same 2-dimensional distribution for $\lvert Q_L\rvert < 2$ MeV/c and $Q_T < 4$ MeV/c with the same free fit parameters (Table 4). After subtracting the background in the low Q region, one observes again a statistically significant signal with a shape described by the simulated Q_T distribution of atomic pairs from $A_{2\pi}^L$ breakup in Pt (Figure 11b). The number of atomic pairs in the region $Q_T < 4$ MeV/c is $n_A^L = 429 \pm 56$. This number is less than the above value due to the additional cut $\lvert Q_L\rvert < 2$ MeV/c.

The measurement of the atomic pair number n_A^L is affected by the description accuracy of the simulated distributions for Coulomb, non-Coulomb and atomic pairs. The Coulomb enhancement function $A_C(q)$ (4) for the Coulomb pairs generated in Be varies slowly for the data shown in Figure 10 and 11, as the range of initial relative momentum Q begins from about 11 MeV/c (Section 2). This is far away from the origin, where $A_C(q)$ varies quickly: compare the Coulomb pair shapes in Figures 10 and 9. The non-Coulomb pairs show a uniform distribution of Q_L. Therefore, a systematic error might arise only from an incorrect description of the atomic pair distribution, due to uncertainties in the Q_L and Q_T resolutions [45].

There are two main sources of systematic errors in the number n_A^L of atomic pairs: 1) The Λ width correction accuracy (Section 6) leads to a systematic error of $\sigma_\Lambda^{syst} = 4.4$. 2) The accuracy of the measured Pt foil thickness dominates the uncertainty in the Q_T resolution, causing a systematic error of $\sigma_{Pt}^{\rm syst} = 22$ in the 2-dimensional analysis. In the 1-dimensional $\lvert Q_L\rvert$ analysis, this error is nearly 0. Generation of $\pi^+\pi^-$ pairs by beam halo protons is negligible [23].

Figure 10b shows the difference between the experimental and simulated distributions. The resulting signal spectrum is only moderately described by the simulated distribution of atomic pairs from $A_{2\pi}^L$ breakup. An additional 1-dimensional $\lvert Q_L\rvert$ analysis is performed to check the influence of the simulated atomic pair shape. The experimental distribution is analysed with 3 free parameters (fractions of atomic, Coulomb and non-Coulomb pairs) in the range $0 < \lvert Q_L\rvert < 15$ MeV/c, and with 2 parameters (fractions of Coulomb and non-Coulomb pairs) in the interval $2 < \lvert Q_L\rvert < 15$ MeV/c, where no atomic pairs are expected. For the 2 parameter fit, the background distribution is calculated in whole range ($0 < \lvert Q_L\rvert < 15$ MeV/c) and subtracted from the experimental distribution. In this analysis, the shape of the simulated atomic pairs has no influence. Figure 12 shows the experimental distribution after subtraction of the background calculated with 3 parameters, the simulated distribution of atomic pairs and the experimental distribution after subtraction of the background from the 2-parameter fit. In the region $\lvert Q_L\rvert < 2$, $Q_T < 4$ MeV/c, the atomic pair numbers obtained with the 3-parameter fit are $n_A^L = 435 \pm 103$ and obtained with the 2-parameter fit $n_A^L = 579 \pm 164$ (Table 4). One sees that the shapes of the excess above the

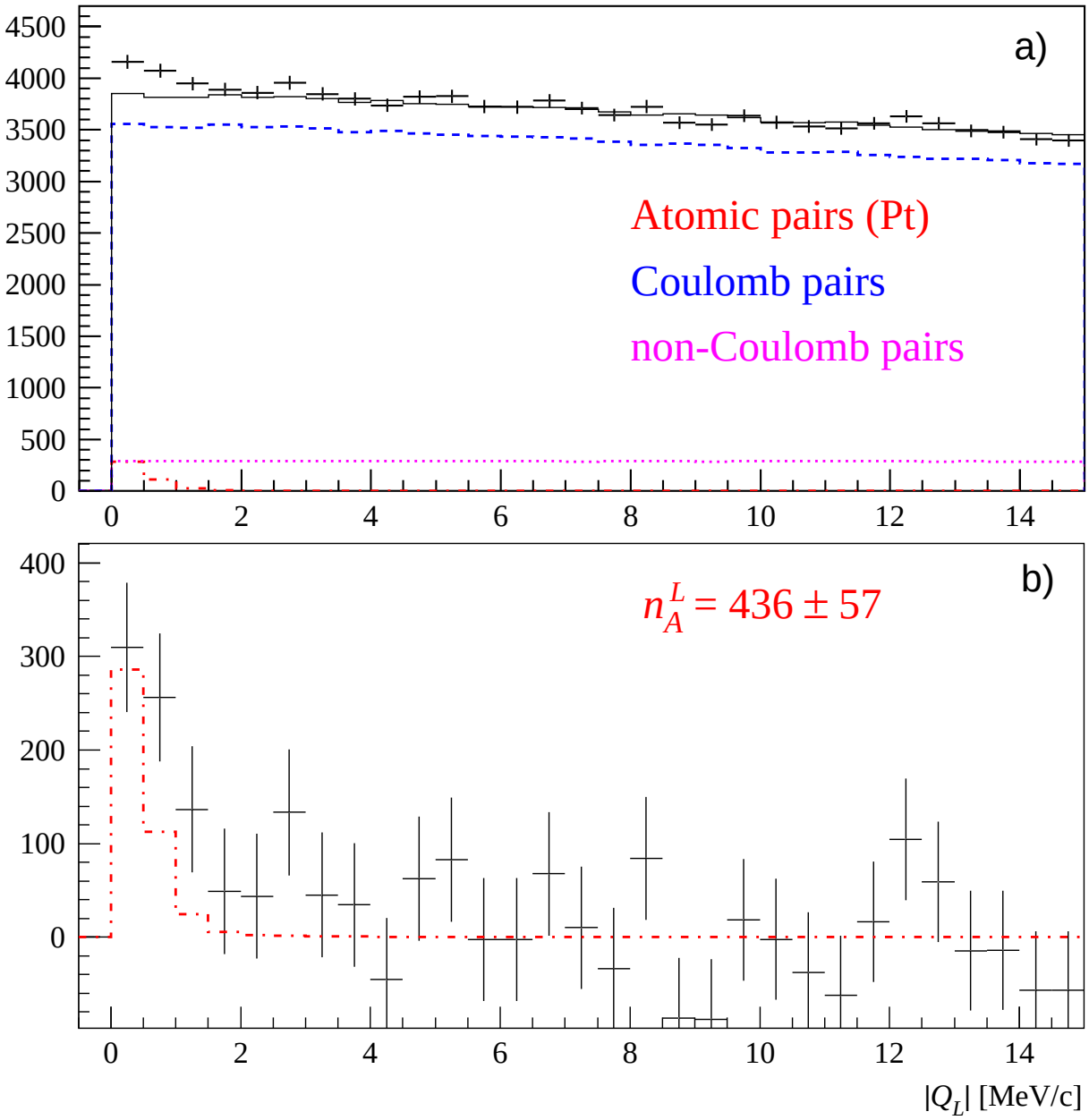

Fig. 10: $|Q_L|$ distribution of $\pi^+\pi^-$ pairs for $Q_T < 2.0$ MeV/c. Plot a) presents the experimental distribution (+ with statistical error bar) and the simulated background (solid line). Plot b) shows the experimental distribution after background subtraction (+ with statistical error bar) and the simulated distribution of atomic pairs from $A_{2\pi}^L$ broken up in Pt (dotted-dashed line). The fit procedure has been applied to the 2-dimensional $(|Q_L|, Q_T)$ distribution.

background distribution are similar. The difference in n_A^L is mainly due to different signal shapes in the experiment and simulation. Statistical fluctuations could be an explanation, because the size of the difference is comparable with the statistical error. Therefore, this difference is taken as an estimate for the systematic error (only with positive sign) $\sigma_{shape}^{syst} = 144$. The systematic error of the number of atoms ($N_A^{\rm tot}$) produced in Be is calculated as maximum difference between the value of the analysis with current variables and other analyses, $\sigma_A^{syst} = 260$.

In summary, the analysis of the 2-dimensional $(|Q_L|, Q_T)$ distributions yields the following value for the

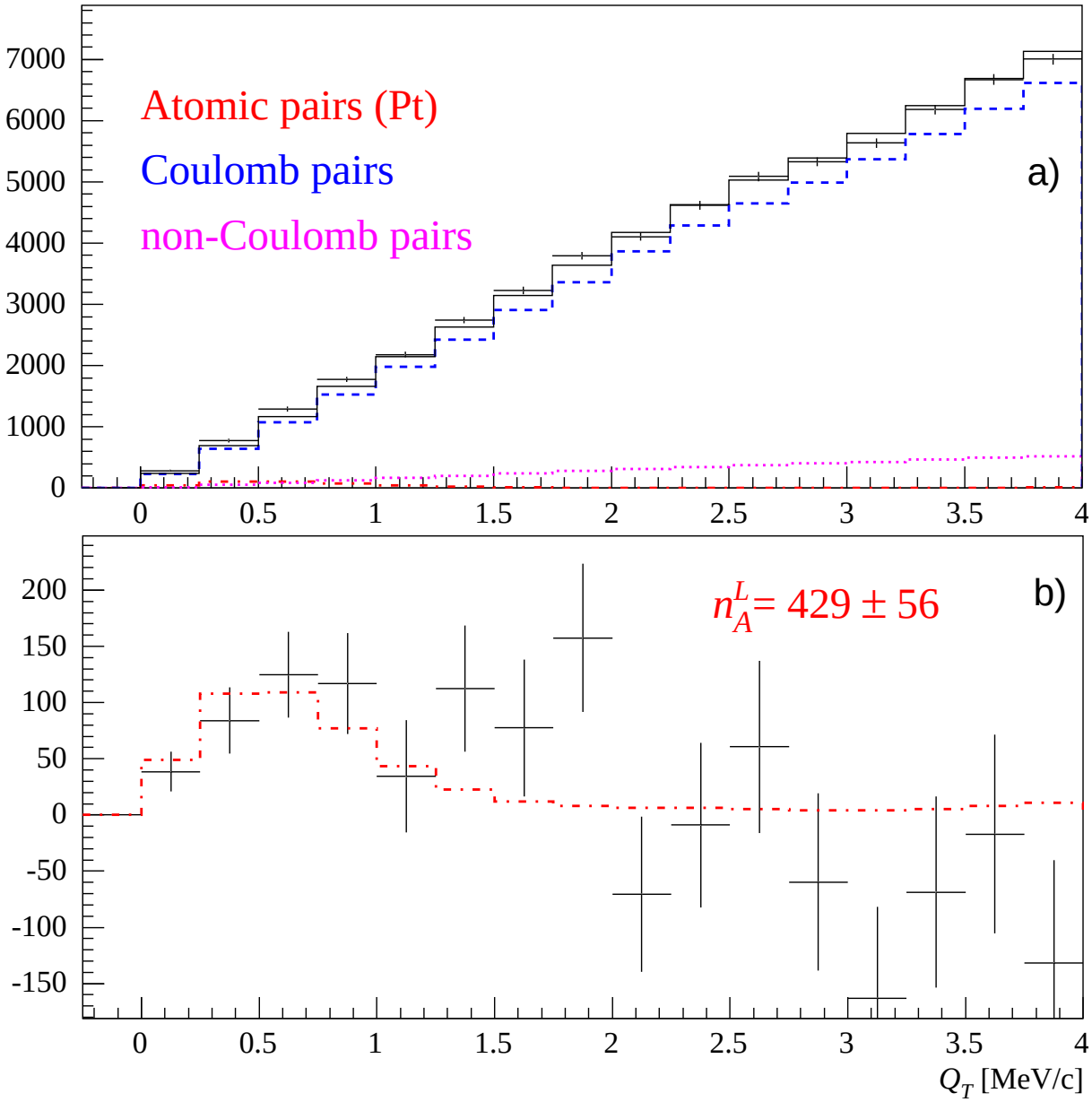

Fig. 11: Q_T distribution of $\pi^+\pi^-$ pairs for $|Q_L| < 2$ MeV/c. Plot a) presents the experimental distribution (+ with statistical error bar) and the simulated background (solid line). Plot b) shows the experimental distribution after background subtraction (+ with statistical error bar) and the simulated distribution of atomic pairs from $A_{2\pi}^L$ broken up in Pt (dotted-dashed line). The fit procedure has been applied to the 2-dimensional ($|Q_L|, Q_T$) distribution.

total probability that a $\pi^+\pi^-$ atom produced in Be breaks up in the Pt foil:

$$P_{\rm br}^{\rm tot}({\rm Pt}) = \frac{n_A^L}{N_A^{\rm tot}} = 0.0257 \pm 0.0034|_{\rm stat}\, {}^{+0.0086}_{-0.0014}|_{\rm syst} = 0.0257^{+0.0092}_{-0.0036}|_{\rm tot}\,. \tag{8}$$

It is crucial that this probability is compatible with the above simplified calculation (6) based on QED lifetimes of long-lived states.

9 Measuring a long-lived $\pi^+\pi^-$ atom lifetime

A long-lived atom lifetime is evaluated by means of two analyses. In the first simplified analysis, all long-lived atoms are considered as objects, which have one common lifetime without accounting for their

Table 4: Different analyses and their conditions. The evaluated numbers n_A^L of atomic pairs are presented with their statistical errors. The following systematical errors are considered: $\sigma_\Lambda^{syst} = \pm 4.4$, $\sigma_{Pt}^{syst} = \pm 22$ and $\sigma_{shape}^{syst} = +144$ (see text).

ΔQ (MeV/c)	n-dim analysis	fit parameter	n_A^L
$\lvert Q_L\rvert < 15, Q_T < 2$	2	3	436 ± 57
$\lvert Q_L\rvert < 2, Q_T < 4$	2	3	429 ± 56
$\lvert Q_L\rvert < 2, Q_T < 4$	1	3	435 ± 103
$\lvert Q_L\rvert < 2, Q_T < 4$	1	2	579 ± 164

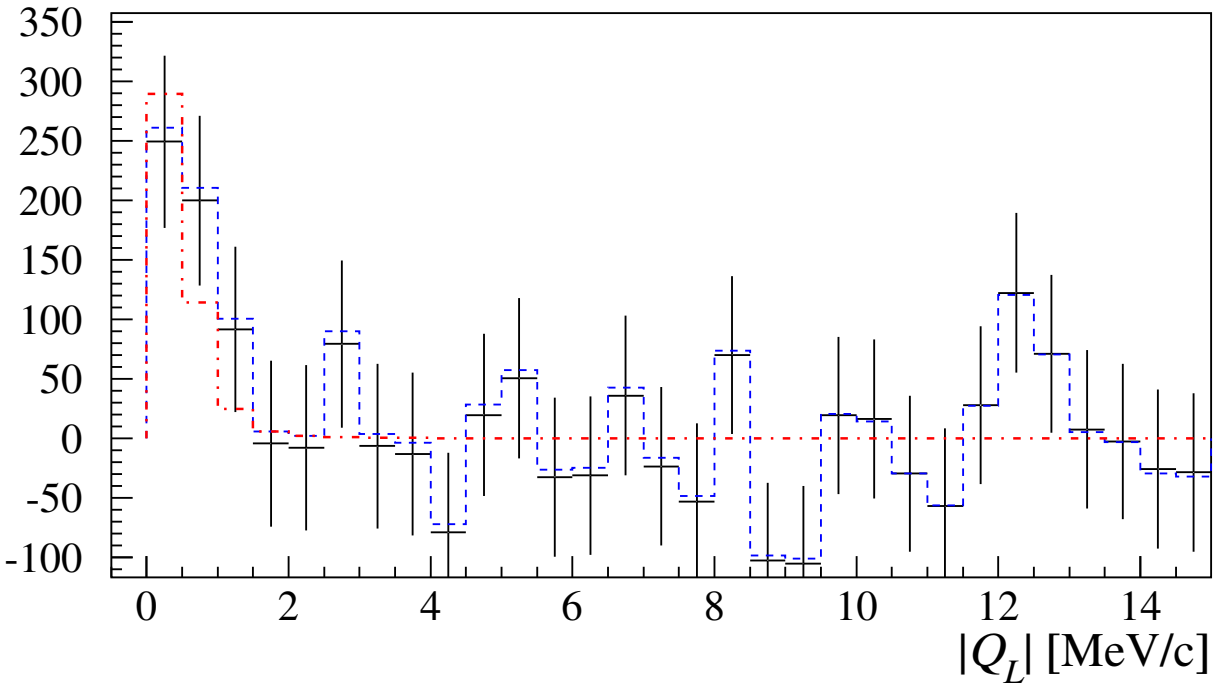

Fig. 12: $|Q_L|$ experimental distribution after subtraction of the background obtained with the 3-parameter fit (+ with statistical error) and after subtraction of the background obtained with the 2-parameter fit (blue dashed line). The distributions are compared to the simulated distribution of atomic pairs (red dotted-dashed line). The fit procedures have been applied to the 1-dimensional $|Q_L|$ distribution.

quantum numbers and any theoretical information about electromagnetic transitions in the atom. Moreover, the breakup probabilities of all $A_{2\pi}^L$ states in the Pt foil are assigned to that of the $8p$ state: 0.9989 (Table 2). Using this value, the measured number of atomic pairs generated in Pt, $n_A^L = 436^{+157}_{-61}\big|_{\rm tot}$, yields a minimum estimated number of long-lived atoms at the Pt entry: $N_A^{L,{\rm Pt}} = 436.5^{+157}_{-61}\big|_{\rm tot}$. The total number of long-lived atoms at the exit of the Be target is $N_A^{L,{\rm Be}} = (6.13^{+0.11}_{-0.09}) \cdot 10^{-2} \times N_A = 1040^{+26}_{-24}\big|_{\rm tot}$. The average momentum of long-lived atoms in the lab system is $\langle p_A \rangle = 4.44$ GeV/c, the Lorentz factor $\gamma = 15.95$ and the velocity βc. Hence, a long-lived atom lifetime τ can be extracted from the relation for an exponential decay with d being the distance between the Be target and the Pt foil: $N_A^{L,{\rm Pt}} = N_A^{L,{\rm Be}} \exp(-d/c\tau\beta\gamma)$. Thus, the minimum the long-lived atom lifetime is estimated to be

$$\tau_{\rm min} = \left(2.32 \pm 0.35|_{\rm stat}{}^{+0.90}_{-0.15}\big|_{\rm syst}\right) \cdot 10^{-11}\,{\rm s} = \left(2.32^{+0.96}_{-0.38}\big|_{\rm tot}\right) \cdot 10^{-11}\,{\rm s}. \quad (9)$$

This value of the long-lived atom lifetime is more than three orders of magnitude larger than our mea-

sured value of the atom ground state lifetime $\tau_{1s} = \left(3.15^{+0.28}_{-0.26}\big|_{\rm tot}\right) \cdot 10^{-15}$ s [3]. The exponential decay is illustrated in Figure 8 by the dashed line. This lifetime can be interpreted as an average lifetime regarding the populations of long-lived states at the exit of the Be target. Thus, its value should be higher than the shortest $2p$ lifetime obtained below. Accounting for the additional calculation errors, discussed in Section 4.1, leads to almost the same value: $\tau_{min} = (2.33^{+0.98}_{-0.39}\big|_{\rm tot}) \cdot 10^{-11}$ s.

In the second more sophisticated analysis, the populations of the pionium states are described in terms of transport equations for the whole path from the production point in the Be target to the exit of the Pt foil. As mentioned above, the interaction of atomic states with material atoms and annihilation of short-lived states are taken into account for the thin solid materials. For the gap between Be and Pt with a length comparable with decay lengths of long-lived states, radiation transition rates and annihilation of short-lived states are included in the transport equations. The variation of the different $A^L_{2\pi}$ lifetimes τ_i from their QED values τ_i^{QED} [43] is done via one common factor $\alpha = \tau_i/\tau_i^{QED}$. All the probabilities involved in these calculations are averaged over the momentum spectrum of the observed atoms (Figure 5).

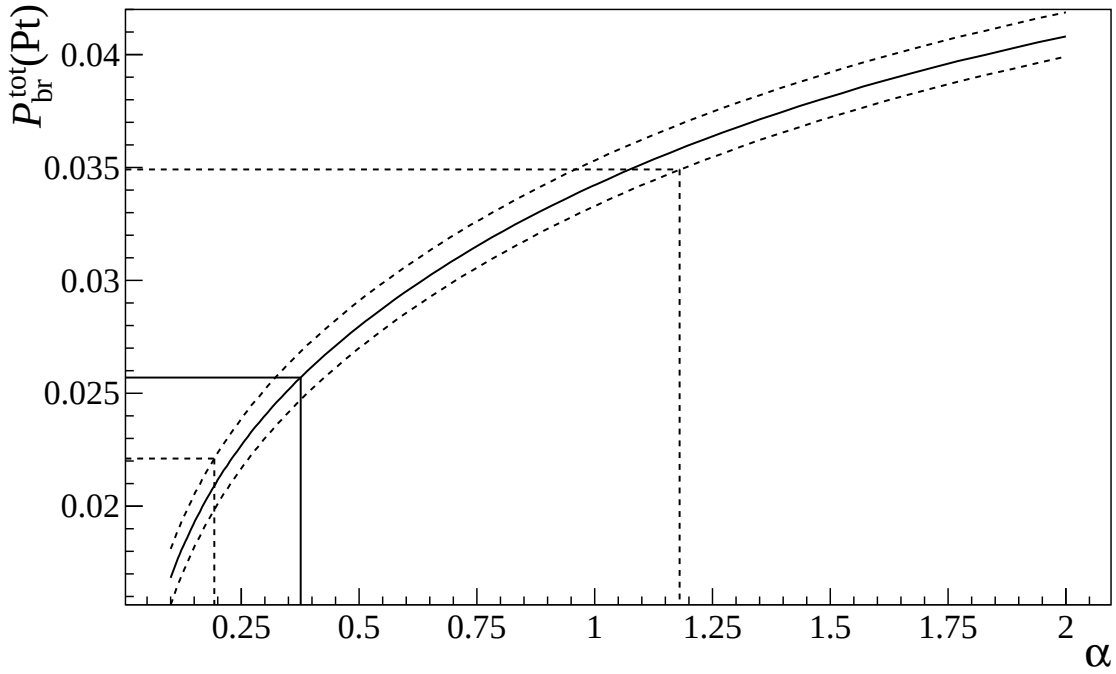

Fig. 13: Probability $P^{\rm tot}_{\rm br}({\rm Pt})$ calculated as a function of α (see text). The horizontal lines correspond to the measured value $P^{\rm tot}_{\rm br}({\rm Pt}) = 0.0257^{+0.0097}_{-0.0036}\big|_{\rm tot}$ (8) together with the total errors. The value $\alpha = 1$, which corresponds to pure QED calculations, is within the error band of the measurement.

The solid line curve in Figure 13 presents the breakup probability in the Pt foil, $P^{\rm tot}_{\rm br}({\rm Pt})$, as a function of the factor α. The error band (dashed curves) accounts for the different extrapolations of the state population for $n \geq 10$ (Section 4). The horizontal lines are the measured value $P^{\rm tot}_{\rm br}({\rm Pt})$ (8) together with the total errors. This value corresponds to $\alpha = 0.376^{+0.804}_{-0.183}$. As $\alpha = 1$ is included in the error band, one concludes that the measured lifetime does not contradict the QED calculations. The lifetime of the $2p$ state, which is the shortest-lived of all long-lived states, is found to be $\tau_{2p} = \left(0.44^{+0.94}_{-0.21}\big|_{\rm tot}\right) \cdot 10^{-11}$ s. This value is in agreement with the calculation in QED, $\tau_{2p} = 1.17 \cdot 10^{-11}$ s.

Accounting for the additional calculation errors, discussed in Section 4.1, leads to a wider error band for $\alpha = 0.383^{+0.926}_{-0.254}$ and the $2p$ lifetime τ_{2p}:

$$\tau_{2p} = \left(0.45^{+1.08}_{-0.30}\big|_{\rm tot}\right) \cdot 10^{-11}{\rm s}\,. \qquad (10)$$

As mentioned in Section 4.2, the magnetic field will decrease the lifetime of the p states with $m = \pm 1$. In Table 1, one can see that the relative number of these states with $n > 3$ is 8.6%. This gives the maximum possible decrease of the long-lived atom population, caused by the magnetic field. In this extreme case, the value of the $2p$ lifetime is $\tau_{2p} = (0.60^{+1.34}_{-0.30}|_{\text{tot}}) \cdot 10^{-11}$ s, not contradicting the result in (10), evaluated without taking intoaccount the influence of the magnetic field.

10 Conclusion

For the first time, a long-lived $\pi^+\pi^-$ atom lifetime has been measured in a dedicated experiment by means of the adapted DIRAC setup. The $\pi^+\pi^-$ pairs are produced by 24 GeV/c protons hitting a 103 μm thick Be target. The analysis of about 320000 Coulomb pairs with small Q yields 16960 ± 130 $\pi^+\pi^-$ atoms in ns states. These atoms move in the target and interact electromagnetically with Be atoms. About 6% of the $\pi^+\pi^-$ atoms leave the target in excited long-lived states and enter the 96 mm gap between the target and the 2.1 μm thick Pt foil. Some of these bound states decay, whereas the rest of about 3.5% get into the Pt foil: more than 90% of these $A^L_{2\pi}$ break up, generating $n^L_A = 436^{+157}_{-61}|_{\text{tot}}$ $\pi^+\pi^-$ atomic pairs.

The first simplified analysis, assuming one common lifetime for all long-lived states, provides an estimate of the minimum $A^L_{2\pi}$ lifetime, $\tau_{\text{min}} = \left(2.33^{+0.98}_{-0.39}|_{\text{tot}}\right) \cdot 10^{-11}$ s. The second more sophisticated analysis takes into account the properties of all pionium atomic states and their populations over the whole path from the production point in the Be target to the exit of the Pt foil. In the analysis, the lifetimes of the long-lived states are varied simultaneously in order to get agreement between the measured number of $\pi^+\pi^-$ pairs from the atom breakup in the Pt foil and the calculated one. One realizes that the measured value does not contradict the calculation with pure QED values of long-lived state lifetimes. The $2p$ lifetime, which is the shortest of all other $A^L_{2\pi}$ lifetimes, is determined as $\tau_{2p} = (0.45^{+1.08}_{-0.30}|_{\text{tot}}) \cdot 10^{-11}$ s. This value is compatible with the QED value $\tau_{2p} = 1.17 \cdot 10^{-11}$ s.

The evaluated lifetime is three orders of magnitude larger than our previously measured value of the $A_{2\pi}$ ground state lifetime $\tau = \left(3.15^{+0.28}_{-0.26}|_{\text{tot}}\right) \cdot 10^{-15}$s [3]. The $A^L_{2\pi}$ observation and the experimental confirmation of the predicted $A^L_{2\pi}$ lifetime open a possibility to measure the *Lamb shift* of this atom and, herewith, a new $\pi\pi$ scattering length combination $2a_0 + a_2$. These scattering lengths have been calculated in the framework of Chiral Perturbation Theory and are nowadays investigated in Lattice QCD.

Acknowledgements

We are grateful to O.V. Teryaev for the useful discussions, A. Vorozhtsov, D. Tommasini and their colleagues from TE-MSC/CERN for the Sm-Co magnet design and construction, R. Steerenberg and the CERN-PS crew for the delivery of a high quality proton beam and the permanent effort to improve the beam characteristics. The project DIRAC has been supported by CERN, the JINR administration, the Ministry of Education and Youth of the Czech Republic by project LG130131, the Istituto Nazionale di Fisica Nucleare and the University of Messina (Italy), the Grant-in-Aid for Scientific Research from the Japan Society for the Promotion of Science, the Ministry of Research and Innovation (Romania), the Ministry of Education and Science of the Russian Federation and Russian Foundation for Basic Research, the Dirección Xeral de Investigación, Desenvolvemento e Innovación, Xunta de Galicia (Spain) and the Swiss National Science Foundation.

References

[1] L. Afanasyev et al., Phys. Lett. B308 (1993) 200.

[2] B. Adeva et al., Phys. Lett. B619 (2005) 50.

[3] B. Adeva et al., Phys. Lett. B704 (2011) 24.

[4] B. Adeva et al., Phys. Lett. B674 (2009) 11.
[5] B. Adeva et al., Phys. Lett. B735 (2014) 288.
[6] B. Adeva et al., Phys. Rev. Lett. 117 (2016) 112001.
[7] B. Adeva et al., Phys. Rev. D96 (2017) 052002.
[8] L. Nemenov, Yad. Fiz. 41 (1985) 980 [Sov. J. Nucl. Phys. 41 (1985) 629].
[9] J. Uretsky and J. Palfrey, Phys. Rev. 121 (1961) 1798.
[10] S.M. Bilenky et al., Yad. Phys. 10 (1969) 812, Sov. J. Nucl. Phys. 10 (1969) 469.
[11] H. Jallouli and H. Sazdjian, Phys. Rev. D58 (1998) 014011,
Erratum: ibid., D58 (1998) 099901.
[12] M.A. Ivanov et al., Phys. Rev. D58 (1998) 094024.
[13] J. Gasser et al., Phys.Rev. D64 (2001) 016008.
[14] G. Colangelo, J. Gasser, H. Leutwyler, Nucl. Phys. B603 (2001) 125.
[15] L. Nemenov and V.D. Ovsyannikov, Phys. Lett. B514 (2001) 247.
[16] L. Nemenov, V.D. Ovsyannikov and E.V. Chaplygin, Nucl. Phys. A 710 (2002) 303.
[17] G.V. Efimov, M.A. Ivanov and V.E. Lyubovitskij, Yad. Fiz. 44 (1986) 460, Sov. J. Nucl. Phys. 44 (1986) 296.
[18] A. Gashi et al., Nucl. Phys. A628 (1998) 101.
[19] J. Schweizer, Phys. Lett. B587 (2004) 33;
J. Schweizer, Eur. Phys. J. C36 (2004) 483.
[20] A. Karimhodjaev and R.N. Faustov, Yad. Fiz. 29 (1979) 463, Sov.J.Nucl. Phys. 29 (1979) 232.
[21] G.J.M. Austen, J.J. de Swart, Phys. Rev. Lett. 50 (1983) 2039.
[22] D. Eiras and J. Soto, Phys. Lett. B491 (2000) 101.
[23] B. Adeva et al., Phys. Lett. B 751 (2015) 12.
[24] B. Adeva et al., CERN-SPSC-2011-001, cds.cern.ch/record/1319290.
[25] B. Adeva et al., Nucl. Instr. Meth. A 839 (2016) 52.
[26] M. Pentia et al., Nucl. Instr. Meth. A 795 (2015) 200.
[27] A. Vorozhtsov et al., DN[1]-2013-04, cds.cern.ch/record/1622178.
[28] G. Gamov, Z. Phys. 51 (1928) 204.
[29] A. Sommerfeld, *Atombau und Spektrallinien* (F. Vieweg & Sohn, 1931).
[30] A.D. Sakharov, Sov. Phys. Usp. 34 (1991) 375.
[31] L. Afanasyev, O. Voskresenskaya, Phys. Lett. B453 (1999) 302.
[32] R. Lednicky, J. Phys. G: Nucl. Part. Phys. 35 (2008) 125109.
[33] R. Lednicky, DIRAC-Note-2012-05; cds.cern.ch/record/1475781.
[34] A. Tarasov and I. Christova, JINR Communication, P2–91–10, Dubna, 1991.
[35] L.G. Afanasyev and A.V. Tarasov, Yad. Fiz. 59 (1996) 2212; Phys. Atom. Nucl. 59 (1996) 2130.
[36] L. Afanasyev et al., J. Phys. B: At. Mol. Opt. Phys. 37 (2004) 4749.
[37] C. Santamarina, M. Schumann, L.G. Afanasyev and T. Heim, J. Phys. B: At. Mol. Opt. Phys. 36 (2003) 4273.
[38] T.A. Heim et al., J. Phys. B: At. Mol. Opt. Phys. 33 (2000) 3583.
[39] T.A. Heim et al., J. Phys. B: At. Mol. Opt. Phys. 34 (2001) 3763.
[40] M. Schumann, et al., J. Phys. B: At. Mol. Opt. Phys. 35 (2002) 2683.
[41] M. Zhabitsky, Physics of Atomic Nuclei 71 (2008) 1040 (arXiv:0710.4416).
[42] M. Zhabitsky, DN-2007-11; cds.cern.ch/record/1369651.

[1] DN=DIRAC-NOTE

[43] V.D. Ovsiannikov, DN-2015-01, cds.cern.ch/record/2012229.
[44] A. Benelli, V. Yazkov, DN-2013-03, cds.cern.ch/record/1622175.
[45] V. Yazkov, DN-2015-02, cds.cern.ch/record/2012230.